



A physics-based flow stress model for cutting simulation of additively manufactured Alloy 718

Downloaded from: <https://research.chalmers.se>, 2026-04-16 05:50 UTC

Citation for the original published paper (version of record):

Malakizadi, A., M'Saoubi, R. (2025). A physics-based flow stress model for cutting simulation of additively manufactured Alloy 718. *CIRP Annals - Manufacturing Technology*, 74(1): 113-117.
<http://dx.doi.org/10.1016/j.cirp.2025.04.024>

N.B. When citing this work, cite the original published paper.



A physics-based flow stress model for cutting simulation of additively manufactured Alloy 718

Amir Malakizadi^{*,a}, Rachid M'Saoubi (1)^{b,c}

^a Department of Industrial and Materials Science, Chalmers University of Technology, Gothenburg, Sweden

^b R&D Materials and Technology, Seco Tools AB, Fagersta, Sweden

^c Division of Production and Materials Engineering, Lund University, Lund, Sweden

ARTICLE INFO

Article history:

Available online 8 May 2025

Keywords:

Modeling
Cutting
Additive manufacturing

ABSTRACT

A dislocation-based flow stress model is proposed to describe the behavior of Alloy 718 fabricated using laser-based and electron-beam powder bed fusion methods. This physics-based model is adaptive to microstructural variations including the size and volume fraction of γ'' precipitates, crystallographic texture, grain size and the density of immobile dislocations. Coupled with data from thermodynamic and kinetic simulations, as well as insights from advanced characterization methods, this model provides a framework for assessing machinability of additively manufactured Alloy 718. The predicted cutting forces and chip shape parameters showed a good agreement with the corresponding measurements.

© 2025 The Author(s). Published by Elsevier Ltd on behalf of CIRP. This is an open access article under the CC BY license (<http://creativecommons.org/licenses/by/4.0/>)

1. Introduction

Additively manufactured (AM) components exhibit a distinctive set of microstructural characteristics that differentiate them from those fabricated by traditional manufacturing processes like casting and forming [1]. These features typically include unique distributions of grain morphology (i.e., size and shape), pronounced crystallographic textures, cellular structures and high dislocation densities. These microstructural properties can evolve throughout the value-chain, influenced by adoption of new AM techniques or modifications to process parameters within a specific AM method. In addition, thermo-mechanical post-treatments, such as aging or hot isostatic pressing (HIP), significantly impact the microstructure of AM components. These changes directly influence the machinability of AM materials, affecting aspects such as tool wear during machining operations [2,3] and/or the surface integrity of finished parts [4]. The intricate interplay between process, microstructure, and properties in additive manufacturing advocates the development of advanced microstructure-sensitive models and methods for prediction of material behavior during machining. Physics-based flow stress models that are adaptive to microstructural variations offer significant advantages over the commonly used phenomenological models, such as the Johnson-Cook model and its modifications [5]. Phenomenological models often require costly experimental recalibration when the microstructural characteristics of the workpiece material change. In contrast, physics-based models are derived from the fundamental understanding of dominant deformation mechanisms, allowing them to remain adaptive to microstructural variations once calibrated. These models have been successfully employed to predict the flow stress properties of various materials, including carbon steels [6], titanium alloys [7], and Ni-based alloys [8].

This study aims to present a physics-based flow stress model that is adaptive to variations in the microstructural characteristics such as grain size, density of immobile dislocations, size and volume fraction of strengthening precipitates and crystallographic texture. These properties are identified either by Electron Backscatter Diffraction (EBSD) technique or advanced kinetic simulations. The key model parameters are initially calibrated using the data available in literature for wrought Alloy 718 [9,10]. Next, the model is extended to predict the flow stress behavior of Alloy 718 produced by two common additive manufacturing processes: laser-based powder bed fusion (PBF-LB) and electron-beam powder bed fusion (PBF-EB). The developed model is then employed in cutting simulations to assess its adaptability to microstructural variations. The Integrated Computational Materials Engineering (ICME) approach presented in this investigation provides a reliable framework for assessing the machinability of additively manufactured Alloy 718.

2. Experimental procedure and microstructural analysis

Prior to machining tests, cylindrical workpieces produced using PBF-LB and PBF-EB methods are subjected to standard AMS 5662 double-aging treatment. The AM process parameters, sample dimensions and the heat treatment recipe are detailed in [2]. Orthogonal cutting tests are performed at a cutting speed of 60 m/min, feed rate of 0.1 mm/rev and 2 mm depth of cut. Uncoated cemented carbide tools (WC-6% Co grade) with two different rake angles of 0° and -10° and a constant clearance angle of 7° are used for the machining tests. The edge radii fall within the range of $25 \pm 2 \mu\text{m}$. The cutting forces are measured by a Kistler 3-axis dynamometer, and the chips are collected for further analysis.

The crystallographic texture, local grain misorientations (kernel average misorientation – KAM), and grain size distributions are obtained by EBSD and presented in [2]. In this study, however, a more detailed analysis is conducted using the MATLAB-based open-

* Corresponding author.

E-mail address: amir.malakizadi@chalmers.se (A. Malakizadi).

source texture analysis toolbox – MTEX (V5.11.2) – to obtain the density of geometrically necessary dislocations (GNDs) and Taylor factor under plane strain condition consistent with assumptions made in 2D Finite Element (FE) simulations.

To incorporate the impact of crystallographic texture into the flow stress model, the Taylor factor is computed by applying the strain tensors to EBSD maps obtained from the surface perpendicular to the build direction. This approach is adopted because material deformation during the orthogonal cutting tests predominantly occurs on the surface encompassing the transverse-normal (TD-ND) directions. Fig. 1a shows the calculated average Taylor factors (M) under the plane strain condition by imposing the tensor $\varepsilon_\theta = \mathbf{R} \times \mathbf{L} \times \mathbf{R}^T$ where \mathbf{L} is a 2nd rank strain tensor while \mathbf{R} and \mathbf{R}^T are the rotation matrix and its transpose, respectively. Similarly, the average grain size is obtained on the surface encompassing TD-ND directions.

GNDs are stored in the strain gradient fields induced by geometrical constraints of the crystal lattice and can thus be quantified by EBSD analysis. Here, the total dislocation line energy minimization method is used to fit the lattice curvature. Initially, the line energy of edge and screw GNDs is determined by conducting a similar analysis on a wrought Alloy 718 sample with a fully recrystallized microstructure, expected to comprise of a total dislocation density of about $5 \times 10^{12} \text{ m}^{-2}$ [11]. Figs. 1b and 1c show the distribution of GNDs in PBF-LB and PBF-EB samples.

In this study, the total dislocation density (ρ) is assumed to be a linear combination of GNDs and statistically stored dislocations. The SSDs have a net-zero Burgers vector; therefore, they cannot be detected by EBSD analysis [12]. However, the complementary X-Ray Diffraction analyses suggested that the ratio between SSDs and GNDs is 1 to 4 [12]. Through a similar approach, the average total dislocation densities (ρ_0) are determined to be $4.07 \times 10^{12} \text{ m}^{-2}$ and $1.39 \times 10^{13} \text{ m}^{-2}$ for PBF-EB and PBF-LB samples, respectively.

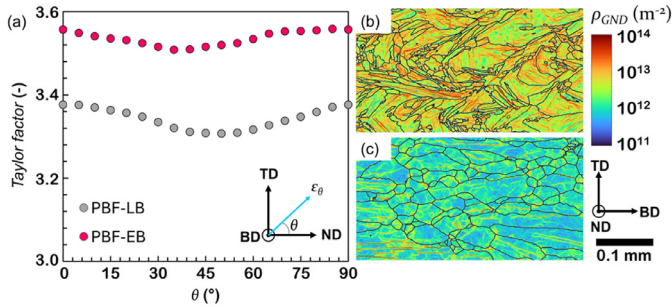


Fig. 1. The average Taylor factor calculated for PBF-LB/Alloy 718 and PBF-EB/Alloy 718 on TD-ND plane parallel to the machining direction (a). Density of GNDs in PBF-LB (b) and PBF-EB (c) samples.

3. Thermodynamic and kinetic simulations

The first step for the estimation of flow stress properties of aged Alloy 718 is to determine the size and volume fraction of the γ' ($\text{Ni}_3(\text{Al}, \text{Ti})$) and γ'' (Ni_3Nb) strengthening precipitates, as well as the concentration of solute atoms in the matrix (γ -phase) contributing to the solid-solution hardening. Here, it was assumed that the major precipitation hardening stems from the coherent and semi-coherent γ'' , while the effect of γ' was neglected. This is because the amount of γ'' in peak-aged Alloy 718 is around 3–4 times larger than that of γ' phase [13] and the misfit between the γ'' precipitates and the matrix is also markedly larger [9]. A similar assumption has been made in previous investigations [8,14].

ThermoCalc[®] software, equipped with TCNI12 and MOBNI6 databases, is used in this study to calculate the equilibrium concentrations of the solute atoms in Alloy 718 during the solutionizing. This is to determine the concentration of Ti, Nb, and Al solute atoms that are not trapped by a more stable δ -phase ($\text{Ni}_3(\text{Nb}, \text{Al}, \text{Ti})$) at the solutionizing temperature (here 954 °C). Given the concentration of major solute atoms in the matrix after solutionizing, the precipitation add-on module to ThermoCalc[®] software, TC-PRISMA[®], is used to estimate the evolution of size and volume fraction of precipitates during the double-aging treatment. Here, the simplified model by Ågren and Chen [15] is adopted to

estimate the growth and dissolution of precipitates. γ'' is simulated as a plate (oblate spheroid) with the aspect ratio of 4, meaning that the ratio between the mean radius (r) and the half thickness (h) of γ'' precipitates is assumed to be 4, in agreement with the experimental observations reported in the literature [16]. Further the matrix was assumed to be isotropic with a shear modulus and Poisson ratio of 57.1 GPa and 0.33, respectively, at the aging temperature. The coherency strain of γ'' is taken as $\varepsilon_{11}^T = \varepsilon_{22}^T = 6.67 \times 10^{-3}$ and $\varepsilon_{33}^T = 2.86 \times 10^{-2}$ [16]. In order to determine the interfacial energy between the matrix and γ'' , a number of simulations are performed to match the experimentally measured mean radii of γ'' precipitates reported by Han et al. [9] after aging the wrought Alloy 718 at various temperatures and dwell times, see Fig. 2. This benchmark resulted in an average interfacial energy of 0.025 J/m² between the matrix and γ'' . These parameters are used hereafter to obtain the volume fraction and dimensions of the γ'' precipitates in the PBF-LB/Alloy 718 and PBF-EB/Alloy 718 after aging treatment.

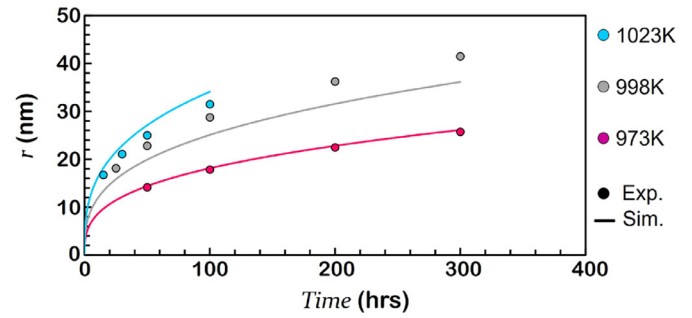


Fig. 2. Simulated and experimentally measured [9] mean radius of γ'' precipitates in wrought Alloy 718 subjected to various aging treatments.

4. Derivation of the physics-based flow stress model

The work hardening in alloys results from the continuous generation and movement of mobile dislocations on the slip plane, and it is significantly influenced by their interactions with the obstacles such as immobile (forest) dislocations, and the stress field imposed by solute atoms, precipitates, and defects in the crystal lattice. Therefore, the flow stress (σ) of alloys may be predicted in an additive manner, taking into account the contributions from the dislocation-obstacle interactions [8]:

$$\sigma = \sigma_0 + \sigma_s + \sigma_{H-P} + \sigma_P + \sigma_G \quad (1)$$

where σ_0 accounts for the short-range interactions of the dislocation core structure with the obstacles of various types in the atomistic scale, often referred to as the Peierls-Nabarro or lattice friction stress, σ_s is the solid-solution strengthening effect, σ_{H-P} is Hall-Petch stress accounting for grain boundary strengthening effects, σ_P is the stress required for the mobile dislocations to bow/bypass or shear the strengthening precipitates, and σ_G is the athermal stress due to, for example, disturbances in the lattice structure and by forest dislocations, i.e. the immobile dislocations on the secondary slip systems obstructing the movement of mobile dislocations on the active slip system.

The lattice friction stress in Eq. 1, σ_0 , can be estimated by [8,17]:

$$\sigma_0 = \tau_0 G \left(1 - \left(\frac{kT}{\Delta f_0 G b^3} \ln \left(\frac{\dot{\varepsilon}_{ref}}{\dot{\varepsilon}_p} \right) \right)^{\frac{1}{q}} \right)^{\frac{1}{p}} \quad (2)$$

where k is the Boltzmann constant, and τ_0 , Δf_0 , p and q are the model constants, and their values are determined against the experimental flow stress data under various temperatures and strain rates ($\tau_0 = 6 \times 10^{-3}$, $\Delta f_0 = 0.51$, $p = 0.85$, and $q = 2.4$). $\dot{\varepsilon}_{ref}$ is the reference strain rate, often taken as $1 \times 10^6 \text{ s}^{-1}$ for fcc materials [17]. G is the temperature dependent shear modulus, T is temperature in Kelvin, and $b = 2.5 \times 10^{-10} \text{ m}$ is the Burgers vector in fcc crystal structure.

The solid-solution strengthening contribution (σ_s) in Eq. 1 is estimated by a Labusch-type model extended for multi-component alloy systems with two or more solute elements [18]:

$$\sigma_s = \left(\sum_i B_i^{3/2} x_i \right)^{2/3} ; B_i = ZMG\Delta_i^{4/3} \quad (3)$$

where x_i is the concentration of solute atom i (in atom fraction), Z is a calibration parameter and determined against the experimental flow stress data ($Z=2 \times 10^{-3}$), and M is the Taylor factor. λ_i is a parameter that accounts for lattice and shear modulus misfits introduced by the solute atom. λ_i can be estimated using the method described in [18] once the shear modulus and atomic radii of the solvent (Ni) and solute atoms (Fe, Cr, Mo and Nb) are known. The Hall-Petch stress (σ_{H-P}) that accounts for grain boundary strengthening effect is also included through:

$$\sigma_{H-P} = k_{HP} \frac{G}{G_0} \frac{1}{\sqrt{d}} \quad (4)$$

with $k_{HP}=750 \text{ MPa}\sqrt{\mu\text{m}}$ taken from the literature [17], d is the grain size and G_0 is the shear modulus of Alloy 718 at 298 K. In order to obtain σ_p , atomic order strengthening due to antiphase boundaries (σ_{P-O}) and coherency-strain strengthening caused by the strain field around coherent and semi-coherent precipitates (σ_{P-C}) are included by the mean square law [13]:

$$\sigma_P = \sqrt{(\sigma_{P-O})^2 + (\sigma_{P-C})^2} \quad (5)$$

The coherency-strain hardening owing to the γ'' precipitates hindering the motion of edge dislocations on the glide plane is estimated based on the model proposed by Oblak et al. [19]:

$$\sigma_{P-C} = \Phi MG|\epsilon|^{3/2} \left(h^2 \frac{f}{3br} \right)^{1/2} \quad (6)$$

where r and h are the mean radius and half-thickness of the disc-shape (oblate) precipitates, respectively. Φ is a calibration parameter ($\Phi=0.6$), ϵ is the misfit parameter associated with the γ'' precipitates ($\epsilon=\epsilon_{33}^T=2.86 \times 10^{-2}$), and f is the volume fraction of γ'' precipitates. Oblak et al. [19] also proposed an equation to estimate the atomic-order strengthening, given as:

$$\sigma_{P-O} = YM \frac{\Gamma_{APB}}{2b} \left[\left(\frac{8f\Gamma_{APB}}{\pi Gb^2} \right) \left(\frac{\sqrt{6}rh}{3} \right)^{1/2} \right]^{1/2} - \frac{f}{3} \quad (7)$$

In the above equation, Γ_{APB} represents the antiphase boundary energy, the value of which is determined by Chaturvedi and Han [13] as 0.296 J/m^2 for γ'' precipitates on the glide plane in Alloy 718, and Y is a calibration parameter ($Y=0.7$).

Lastly, σ_G can be described by the well-known Taylor hardening equation:

$$\sigma_G = \alpha M G b \sqrt{\rho} \quad (8)$$

where ρ is the total density of immobile dislocations (here it is assumed that $\rho=\rho_{GND}+\rho_{SSD}$), and $\alpha=1$ is a constant. The immobile dislocations are constantly generated (stored) and annihilated/remobilized during material deformation. The evolution rate of immobile dislocations ($\dot{\rho}$) is influenced by various hardening (+) and recovery (-) contributions:

$$\dot{\rho} = \dot{\rho}^{(+)} - \dot{\rho}^{(-)} \quad (9)$$

The rate of dislocation storage ($\dot{\rho}^{(+)}$) depends on the mean free path (Λ) of mobile dislocations [8]:

$$\dot{\rho}_i^{(+)} = \frac{M}{b} \frac{1}{\Lambda} \dot{\epsilon}_p \quad (10)$$

where $\dot{\epsilon}_p$ is the plastic strain rate. Λ is influenced by dislocation-dislocation and dislocation-obstacle interactions. Here, the mean free path of mobile dislocations is assumed to be controlled collectively by the dislocation-dislocation interactions in the pure substance (Λ_{pure}), dislocation-solute interactions (Λ_{ss}) in the presence of solute atoms, grain boundaries and dislocation cells, and the γ'' precipitates on the glide plane. $1/\Lambda$ in Eq. 10 can then be formulated as follows [8,20]:

$$\frac{1}{\Lambda} = (\zeta_0 + \zeta_{ss} + \zeta_c) \sqrt{\rho} + \frac{\zeta_d}{d} + \frac{\zeta_p}{l_p} \quad (11)$$

where ζ_c , ζ_d and ζ_p are the constants taking the values 2.2×10^{-3} , 1×10^{-3} and 4×10^{-4} , respectively, after the model calibration. $l_p = r \sqrt{2\pi/3f}$ is the mean distance between the precipitates on the glide plane with r as their mean radius and f as their volume fraction,

determined by kinetic calculations. ζ_{ss} is postulated to be [20]:

$$\zeta_{ss} = \frac{\sum x_i}{1.2 \times 10^5} \exp\left(\frac{-\Delta G_{sys}}{RT}\right) \quad (12)$$

with x_i the atom fraction of the major alloying elements (Fe, Cr, Nb and Mo) in the matrix, T , R is the universal gas constant ($R=8.314 \text{ J/mol.K}$) and ΔG_{sys} is the Gibbs energy of the system in J/mol obtained using ThermoCalc® at a given temperature. ζ_0 is also presented as $\zeta_0 = (G/G_0)^2/300$.

The rate of dislocation dynamic recovery ($\dot{\rho}^{(-)}$) in Eq. 9 is assumed to be controlled solely by the dislocation glide and formulated based on the Orowan postulation as:

$$\dot{\rho}^{(-)} = \Omega \rho \dot{\epsilon}_p \quad (13)$$

where Ω is a temperature dependent parameter given by [17]:

$$\Omega = \Omega_0 + \Omega_{r0} \left(\frac{D}{b^2 \dot{\epsilon}_p} \right)^{1/3} \quad (14)$$

Here, Ω_0 and Ω_{r0} are the calibration parameters ($\Omega_0=7.8$ and $\Omega_{r0}=0.1$), and $D = D_0 \exp(-Q/RT)$ is a diffusivity coefficient with $D_0=1.6 \times 10^{-4} \text{ m}^2/\text{s}$ as the lattice self-diffusion coefficient of γ -phase [17] and $Q=190 \times 10^3 \text{ J/mol}$ is a calibration parameter determined against the experimental flow stress data at different temperature and strain rates.

Fig. 3a shows experimental flow stress data under given temperatures and strain rates obtained by Split-Hopkinson Pressure Bar (SHPB) test for wrought Alloy 718 – solutioned at 954°C for one hour and aged at 760°C for 5 hours, cooled to 649°C in 2 hours and then held at this temperature for an hour before cooling to the room temperature [10]. This figure also shows the simulated flow stresses at the corresponding temperatures and strain rates using the physics-based model. To determine the model parameters, an optimization algorithm is implemented to minimize the difference (i.e., absolute error) between experimental and simulated flow stresses. Fig. 3b shows the contribution of various deformation mechanisms on the yield stress (σ_y) of wrought Alloy 718 under the conditions shown in Fig. 3a.

The radial return algorithm [21] is used here to determine the effective plastic strain increment, provided that the one-dimensional stress state prevails in SHPB test. This algorithm requires the calculation of the yield stress (σ_y) and hardening modulus (H) to be able to iteratively update the internal state variable (effective plastic strain, $\bar{\epsilon}_p$, and total density of immobile dislocations, ρ). The hardening modulus is defined as:

$$H = \frac{d\sigma_y}{d\bar{\epsilon}_p} = \frac{d\sigma_y}{d\rho} \frac{d\rho}{d\bar{\epsilon}_p} \quad (15)$$

An implicit approach is applied here to estimate ρ by solving Eq. 9 using Newton-Raphson method in a nested loop with the plastic strain increment ($\Delta\bar{\epsilon}_p$) and the time step (Δt) as inputs [17].

To correctly predict the thermal softening behavior of Alloy 718, it is vital to estimate the amount and size of γ'' precipitates under the

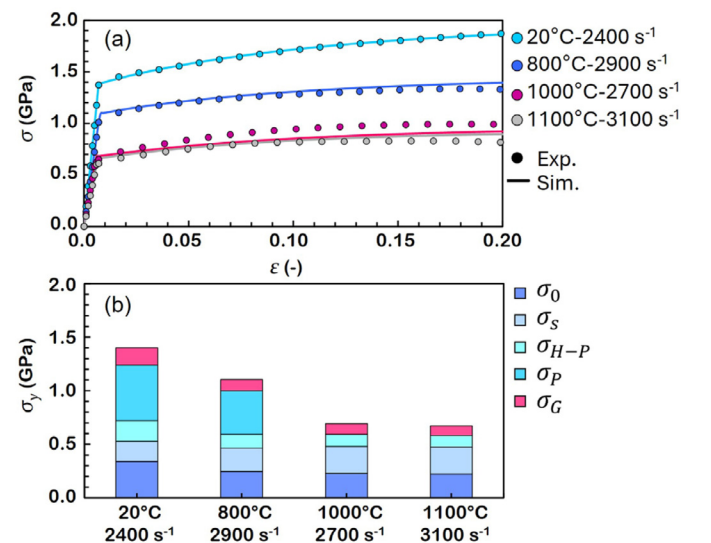


Fig. 3. Simulated and experimentally measured [10] flow stress of wrought Alloy 718 at various strain rates and temperatures (a), the contribution of various deformation mechanisms on σ_y at corresponding conditions (b).

conditions used for SHPB experiments. Here, the amount and size of the precipitates are estimated using TC-PRISMA[®] under the pseudo-equilibrium condition, assuming that all samples were maintained at the aimed temperatures for approximately 50 s before compression [10]. Fig. 4 shows the estimated size and volume fraction of γ'' precipitates at different soaking temperatures. As evident in Figs. 3b and 4, the precipitation hardening effect is completely eliminated at temperatures exceeding the solubility limit of γ'' , and thereafter, the dissolved Nb in the matrix contributes to solid-solution strengthening.

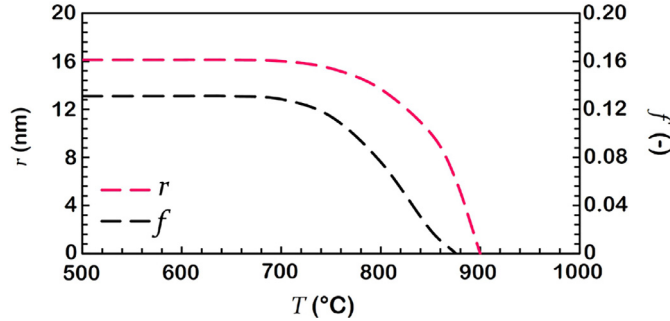


Fig. 4. Estimated mean radius (r) and volume fraction (f) of γ'' precipitates.

5. Evaluation of physics-based model

Cutting simulations are performed to evaluate the performance of the present physics-based model for the prediction of chip shape parameters and the cutting forces when machining PBF materials using tools with two different rake angles (0° and -10°). Here, the calibrated model presented in Section 4 is utilized to predict the flow stress properties of additively manufactured (AM) materials by providing their microstructural attributes as input parameters. SFTC DEFORM 2D[®] is used for the cutting simulations, where the flow stress data at different strain rates and temperatures – generated by an in-house MATLAB-based programme – are imported as the tabulated data. The sliding friction model ($\mu=0.3$) and a perfect thermal condition are assumed to mimic the tribological conditions at the tool-chip interface. A modified Cockcroft and Latham damage model (with 1600 MPa for damage initiation and 65% damage softening) implemented using a Fortran subroutine [22] is applied to simulate serration during chip formation. The friction and damage parameters are selected to minimize the discrepancy between experimental and simulated cutting forces and chip parameters when machining PBF-LB/Alloy 718 using the tool with -10° rake angle. These parameters are then held constant for all other conditions. The size and amount of γ'' precipitates – predicted based on the exact material compositions and heat treatment recipe – as well as the Taylor factor and the estimated total density of dislocations are used as input to the calibrated model presented in Section 4 for predicting the flow stress data for each AM material. Fig. 5 shows the predicted flow stress behaviors at three different temperatures under a given strain rate. As evident, the physics-based model estimates a slightly higher yield stress for PBF-LB/Alloy 718 followed by a more rapid recovery as compared to those of PBF-EB/Alloy 718. A higher yield stress is essentially associated with a higher dislocation density and smaller grain size in PBF-LB/Alloy 718, whereas a higher recovery in this material is due to its smaller Taylor factor. No significant difference is noted between the size and volume fraction of precipitates in these workpiece materials.

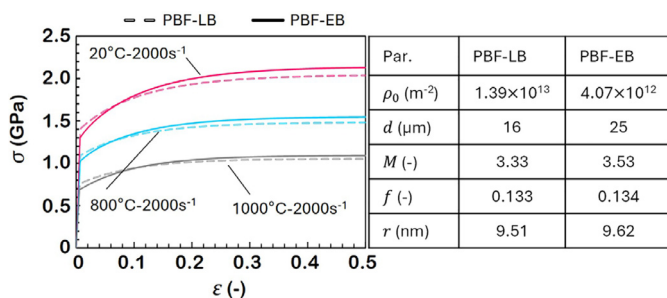


Fig. 5. Estimated flow stress properties for PBF-LB/Alloy 718 and PBF-EB/Alloy 718. ρ_0 is the initial density of immobile dislocations. M is averaged for shear angles within a range between 15° and 35° .

Fig. 6 shows the predicted cutting forces and chip thickness parameters. A good agreement is seen between the predicted and experimental chip formations; however, the simulated forces are systematically lower than the experimental values (16% in cutting force and up to 29% in feed force). The simulation results would be further improved by implementing more advanced friction and damage models as well as a model accounting for dynamic recrystallization to be examined in our future endeavors.

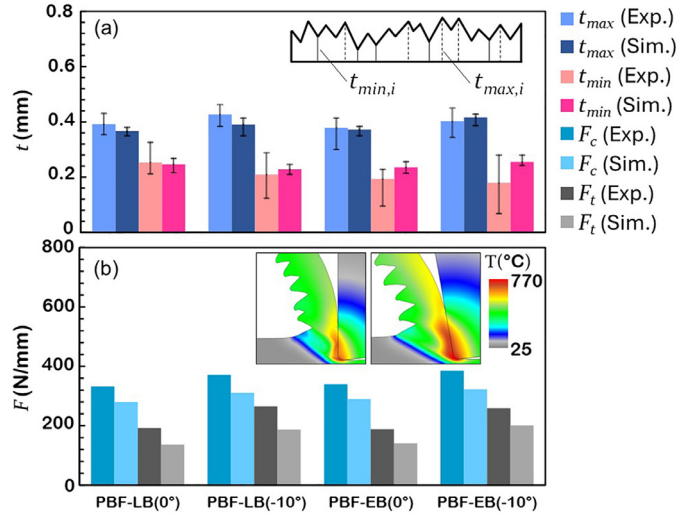


Fig. 6. Simulated and experimental chip thickness (a) and cutting forces (b). The temperature results in this figure are shown for PBF-EB/Alloy 718. Variations in experimental force measurements were within ± 10 N/mm.

6. Summary and outlook

This study presented a physics-based approach to simulate the flow stress behavior of additively manufactured (AM) Alloy 718. The approach integrates advanced thermodynamic and kinetic simulations, comprehensive material characterization data, and a dislocation-based flow stress model that accounts for the variations in the microstructural property driven by different manufacturing processes. A feature of this methodology is its general applicability, enabling the calibrated models to reliably predict the material behavior in machining. The presented ICME approach can be extended for other groups of materials, facilitating the value-chain optimization to attain improved processes and enhanced material performance.

Declaration of competing interest

The authors declare that they have no known competing financial interests or personal relationships that could have appeared to influence the work reported in this paper.

CRediT authorship contribution statement

Amir Malakizadi: Writing – original draft, Visualization, Validation, Software, Project administration, Methodology, Investigation, Funding acquisition, Formal analysis, Data curation, Conceptualization. **Rachid M'Saoubi:** Writing – review & editing, Writing – original draft, Validation, Resources, Methodology.

Acknowledgements

This research was jointly supported by Vinnova (Sweden's Innovation Agency) under the Eureka Smart programme (BRAVE project: 2023–02528) and Swedish Foundation for Strategic Research (grant no APR20–0029). The support received from the Chalmers Centre for Metal Cutting Research (MCR) and Competence Centre for Additive Manufacturing – Metal (CAM2) is acknowledged. The authors would also like to express gratitude to Per Alm (Seco Tools AB) for helping with the cutting experiments.

References

- [1] Malakizadi A, Mallipeddi D, Dadbakhsh S, M'Saoubi R, Krajnik P (2022) Post-processing of additively manufactured metallic alloys – A review. *International Journal of Machine Tools and Manufacture* :103908.
- [2] Malakizadi A, et al. (2021) The role of microstructural characteristics of additively manufactured Alloy 718 on tool wear in machining. *International Journal of Machine Tools and Manufacture* 171:103814.
- [3] Betts J, Glanvill S, Shokrani A (2024) Impact of directionality and heat treatment on machining of additively manufactured Inconel 718. *CIRP Annals* 73(1):69–72.
- [4] Weng J, et al. (2024) On machining-induced surface integrity of Inconel 718 fabricated by powder bed fusion. *Journal of Materials Processing Technology* 328:118406.
- [5] Melkote SN, et al. (2017) Advances in material and friction data for modelling of metal machining. *CIRP Annals* 66(2):731–754.
- [6] Saez-de-Buruaga M, Aristimuño P, Soler D, D'Eramo E, Roth A, Arrazola PJ (2019) Microstructure based flow stress model to predict machinability in ferrite–pearlite steels. *CIRP Annals* 68(1):49–52.
- [7] Melkote SN, Liu R, Fernandez-Zelaia P, Marusich T (2015) A physically based constitutive model for simulation of segmented chip formation in orthogonal cutting of commercially pure titanium. *CIRP Annals* 64(1):65–68.
- [8] Fisk M, Ion JC, Lindgren L-E (2014) Flow stress model for IN718 accounting for evolution of strengthening precipitates during thermal treatment. *Computational materials science* 82:531–539.
- [9] Han Y-f, Deb P, Chaturvedi MC (1982) Coarsening behaviour of γ'' - and γ' -particles in Inconel alloy 718. *Metal Science* 16A(12):555–562.
- [10] Moretti MA, et al. (2021) High strain rate deformation behavior and recrystallization of alloy 718. *Metallurgical and Materials Transactions A* 52(12):5243–5257.
- [11] Muránsky O, Balogh L, Tran M, Hamelin CJ, Park JS, Daymond MR (2019) On the measurement of dislocations and dislocation substructures using EBSD and HRSD techniques. *Acta Mater* 175:297–313.
- [12] Cui L, et al. (2022) A new approach for determining GND and SSD densities based on indentation size effect: an application to additive-manufactured Hastelloy X. *Journal of Materials Science & Technology* 96:295–307.
- [13] Chaturvedi MC, Han Y-f (1983) Strengthening mechanisms in Inconel 718 superalloy. *Metal Science* 17(3):145–149.
- [14] Balan A, et al. (2021) Precipitation of γ'' in Inconel 718 alloy from microstructure to mechanical properties. *Materialia* 20:101187.
- [15] Ågren J, Chen Q (2022) Simplified growth model for Multicomponent systems - inclusion of PARA and NPLE conditions. *Journal of Phase Equilibria and Diffusion* 43(6):738–744.
- [16] Devaux A, et al. (2008) Gamma double prime precipitation kinetic in Alloy 718. *Materials Science and Engineering: A* 486(1):117–122.
- [17] Malmelöv A, Fisk M, Lundbäck A, Lindgren L-E (2020) Mechanism based flow stress model for alloy 625 and alloy 718. *Materials (Basel)* 13(24):5620.
- [18] Malakizadi A, Saelzer J, Berger S, Alammari Y, Biermann D (2023) A physics-based constitutive model for machining simulation of Ti-6Al-4V titanium alloy. *Procedia CIRP* 117:335–340.
- [19] Oblak JM, Paulonis DF, Duvall DS (1974) Coherency strengthening in Ni base alloys hardened by DO22 γ' precipitates. *Metallurgical transactions* 5(1):143–153.
- [20] Galindo-Nava EI, Rivera-Díaz-del-Castillo PEJ (2013) Thermostatistical modelling of hot deformation in FCC metals. *International Journal of Plasticity* 47:202–221.
- [21] Simo JC, Taylor RL (1986) A return mapping algorithm for plane stress elastoplasticity. *Int J Numer Methods Eng* 22(3):649–670.
- [22] Razanica S, Malakizadi A, Larsson R, Cedergren S, Josefson BL (2019) FE modeling and simulation of machining Alloy 718 based on ductile continuum damage. *International Journal of Mechanical Sciences* :105375.